

Quantum dimensions from local operator excitations in the Ising model

Paweł Caputa¹ and Marek M. Rams²

¹*Nordita, KTH Royal Institute of Technology and Stockholm University,
Roslagstullsbacken 23, SE-106 91 Stockholm, Sweden*

²*Institute of Physics, Jagiellonian University, Łojasiewicza 11, 30-348 Kraków, Poland*

We compare the time evolution of entanglement measures after local operator excitation in the critical Ising model with predictions from conformal field theory. For the spin operator and its descendants we find that Rényi entropies of a block of spins increase by a constant that matches the logarithm of the quantum dimension of the conformal family. However, for the energy operator we find a small constant contribution that differs from the conformal field theory answer equal to zero. We argue that the mismatch is caused by the subtleties in the identification between the local operators in conformal field theory and their lattice counterpart. Our results indicate that evolution of entanglement measures in locally excited states not only constraints this identification, but also can be used to extract non-trivial data about the conformal field theory that governs the critical point. We generalize our analysis to the Ising model away from the critical point, states with multiple local excitations, as well as the evolution of the relative entropy after local operator excitation and discuss universal features that emerge from numerics.

I. INTRODUCTION

The physics of many 1+1 dimensional lattice models at criticality is captured in the continuum limit by two-dimensional conformal field theory (2d CFT). As a result, one can numerically extract the conformal data, for instance scaling dimensions of the primary operators from the scaling of the two-point correlation functions in the critical lattice model, see [1] for the standard reference. On the other hand, measures of entanglement proved to be useful quantities for exploring the critical points of many-body systems. For example, in the ground state of a critical chain, the entanglement entropy of a block of spins has a universal logarithmic scaling with the size of the block that is proportional to the central charge [2]. This provides an efficient numerical way to obtain the central charge of the CFT that governs the critical point, see Refs. [3] for review. It is then natural to ask if entanglement measures in excited states can be used to extract more CFT data, such as for instance the modular S or T matrices or quantum dimensions, numerically.

In rational CFTs local elementary excitations are catalogued into finite number of conformal families containing primary operators and their descendants. The simplest excited states can then be obtained by inserting local CFT operators at some spatial points. In such states, one can study how the local operator changes the structure of entanglement in the ground state. More precisely, it is possible to compute the time evolution of the change in Rényi entropies for a reduced density matrix of a single interval due to the operator insertion [4] – see Ref. [5, 6] for some results in various CFT setups and Ref. [7] for entanglement in a related class of globally excited states. In 2d CFT this analysis can be performed analytically and Rényi entropies detect an increase in entanglement equal to the logarithm of the quantum dimension of the conformal family [8–10].

Having such a clear and elegant prediction from the CFT, it is then natural to wonder if and how the logarithms of quantum dimensions are reproduced on the lattice. In this article we initiate such program for the simplest case of the critical Ising chain. The advantage of the Ising model is that it is exactly solvable and the action of a family of local operators can be efficiently simulated for large system sizes. The main subtle point of this analysis is the identification between the CFT operators and their lattice counterpart. In fact, there are only few models where such map is well established – see for instance the discussion in [11] – and a general belief is that a given lattice operator corresponds in the continuum to a primary operator plus its descendants. In the case of the two-point functions these extra contributions from descendants lead to corrections that are suppressed as higher powers with the distance. In this work, given a well established identification for the Ising model operators, we will be able to check the contribution from this non-unique identification to the physics of entanglement propagation. We will see that for truly local operators on the lattice – like the Ising spin – we recover the CFT answer, but for operators

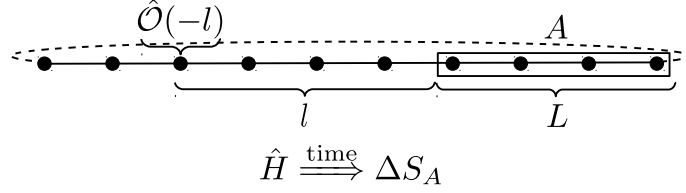


FIG. 1. Schematic illustration of the protocol. Local operator \hat{O} is inserted at a distance l from the block A of L spins. We then calculate the change of entropy of the block ΔS_A resulting from the insertion as a function of time.

with non-local support – like Ising energy – the subleading contributions modify the leading answer and lead to a mismatch.

The computations of Rényi entropies in CFT are done using the replica method that, for excited states, boils down to calculation of correlation functions on complicated Riemann surfaces. Even for states locally excited by more than a single operator such objects are notoriously difficult to compute analytically and features of entanglement measures in this class of states remain unexplored. Similarly, measures of distance between quantum states like, e.g., relative entropy for locally excited states require the access to higher-point correlators [12]. In this work, we will further explore the Ising model to shed a new light in these directions by numerically performing the time evolution of the relative entropy, as well as Rényi entropies in more general states excited by multiple local operators.

This paper is organized as follows. In section II we summarize the relevant results from the two dimensional CFT. In section III we present our main numerical results for the evolution of entanglement in the critical Ising model in states excited by single local operators. In section IV we consider the evolution away from the critical point, as well as more general operator excitations. In section V we present the evolution of the relative entropy after local operator excitation in this model. Finally, we conclude and present the details of our numerical approach in the Appendix A.

II. CFT RESULTS

In this section we briefly review the existing results for the evolution of Rényi entropies in locally excited states in 2d CFTs and then show some details of the computation for the Ising CFT. Finally, we discuss the minor modifications that appear for the CFTs on the cylinder that, in the following sections, we will be comparing to numerics from the periodic chain.

Let us start with a 2d CFT on the real line and a state excited by a local operator $\hat{O}(-l)$ at distance l from the entangling interval $A \in [0, L]$, as presented pictorially on Fig. 1. The density matrix is given by

$$\begin{aligned} \hat{\rho}(t) &= \mathcal{N} \cdot e^{-i\hat{H}t} e^{-\epsilon\hat{H}} \hat{O}(0, -l) |0\rangle \langle 0| \hat{O}^\dagger(0, -l) e^{-\epsilon\hat{H}} e^{i\hat{H}t} \\ &\equiv \mathcal{N} \cdot \hat{O}(w_2, \bar{w}_2) |0\rangle \langle 0| \hat{O}^\dagger(w_1, \bar{w}_1), \end{aligned} \quad (1)$$

where the insertion points of the local operators are defined as

$$\begin{aligned} w_1 &= i(\epsilon - it) - l, & w_2 &= -i(\epsilon + it) - l, \\ \bar{w}_1 &= -i(\epsilon - it) - l, & \bar{w}_2 &= i(\epsilon + it) - l. \end{aligned} \quad (2)$$

The factor of ϵ is the UV regulator for the local operators and we take $\epsilon \rightarrow 0$ at the end of the computation. The normalization \mathcal{N} ensures that the trace of the density matrix is equal to 1.

Using the replica trick, we can compute how a family of Rényi entropies $S_A^{(n)}$, indexed by integer n , changes due to the local operator insertion. The answer to this question is expressed in terms of the logarithm of the ratio [4]

$$\Delta S_A^{(n)} \equiv \frac{1}{1-n} \log \left[\frac{\langle \hat{O}(w_1, \bar{w}_1) \hat{O}^\dagger(w_2, \bar{w}_2) \cdots \hat{O}^\dagger(w_{2n}, \bar{w}_{2n}) \rangle_{\Sigma_n}}{\left(\langle \hat{O}^\dagger(w_1, \bar{w}_1) \hat{O}(w_2, \bar{w}_2) \rangle_{\Sigma_1} \right)^n} \right], \quad (3)$$

where the correlator in the numerator is computed on the n -sheeted surface Σ_n with cuts on each copy corresponding to interval A , and the two-point function in the denominator is on a single sheet Σ_1 with an interval cut A . For a detailed derivation and further illustrative explanations see [4].

In 2d CFT, one can apply a conformal map from Σ_n to a complex plane and evaluate the correlators explicitly. It turns out that the answer is universal and the increase in the Rényi entanglement entropies is equal to a constant

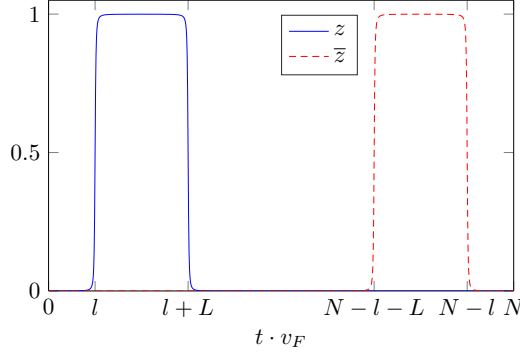


FIG. 2. Evolution of the cross-ratios on the cylinder for a single period of time for small but non-zero ϵ .

that is the same for all the members of a conformal family, i.e. primary operators and their descendants [9, 10]. In rational CFTs this constant is equal to the logarithm of the quantum dimension of the local operator [8] which is defined as

$$d_a = \frac{S_{0a}}{S_{00}}, \quad (4)$$

where S_{ij} denotes the elements of the modular S-matrix of the CFT, see e.g. Ref. [1].

In this work we focus on the 2d Ising model which is the $(4, 3)$ minimal model with three primary operators: the identity $\mathbf{1}$, the energy ε with conformal dimensions $(h_\varepsilon, \bar{h}_\varepsilon) = (\frac{1}{2}, \frac{1}{2})$ ($\Delta_\varepsilon = h_\varepsilon + \bar{h}_\varepsilon = 1$) and the spin σ with $(h_\sigma, \bar{h}_\sigma) = (\frac{1}{16}, \frac{1}{16})$ ($\Delta_\sigma = h_\sigma + \bar{h}_\sigma = \frac{1}{8}$), where $\Delta_{\sigma(\varepsilon)}$ marks the total scaling dimensions.

The modular S-matrix of the Ising model is given by

$$S = \frac{1}{2} \begin{pmatrix} 1 & 1 & \sqrt{2} \\ 1 & 1 & -\sqrt{2} \\ \sqrt{2} & -\sqrt{2} & 0 \end{pmatrix}, \quad (5)$$

so the three quantum dimensions (4) are

$$d_{\mathbf{1}} = d_\varepsilon = 1, \quad d_\sigma = \sqrt{2}. \quad (6)$$

This way, at criticality, only excitations with primary σ can non-trivially change the entanglement in the vacuum state, and for all the Rényi entropies we have [8]

$$\Delta S_A^{(n)} = \log \sqrt{2}. \quad (7)$$

The standard, chiral (anti-chiral) descendants are obtained by either acting on the primary operators with chiral (anti-chiral) derivatives ∂_z ($\bar{\partial}_{\bar{z}}$) or taking the operator product expansion (OPE) of the primary operators with the energy momentum tensor. Such descendants increase the entropies by the same amount as the primaries. If we however act with the linear combination of the two derivatives, there is an additional contribution to the entropy equal to $\log 2$ [10]. We will see this in case of the spatial derivative $\partial_x = \partial_z + \bar{\partial}_{\bar{z}}$ acting on $\sigma(z, \bar{z})$, which we consider in Sec. III C.

In order to compare the CFT results with numerics we have to take into account finite size of the system, N . In the CFT computation it enters through the invariant cross-ratios. Let us, for simplicity, consider the change in the second Rényi entropy $\Delta S_A^{(2)}$ that requires the correlator on two cylinders. The correlators entering (3) are computed using a composition of the conformal map $w(x) = \exp(-\frac{2\pi i}{N}x)$ from each cylinder to the plane with a cut and the uniformization map $z^2(w) = (w-1)/(w-L)$. After some standard CFT manipulations, the change in the entropy can be written as

$$\Delta S_A^{(2)} = -\log(|z(1-z)|^{4h_{\mathcal{O}}} \mathcal{G}_{\mathcal{O}\mathcal{O}}^{\mathcal{O}\mathcal{O}}(z, \bar{z})), \quad (8)$$

where $\mathcal{G}_{\mathcal{O}\mathcal{O}}^{\mathcal{O}\mathcal{O}}$ is the canonical 4-point function on the complex plane with operators \mathcal{O} inserted at $(0, z, 1, \infty)$ and the cross-ratios are defined as

$$z = \frac{z_{12}z_{34}}{z_{13}z_{24}}, \quad \bar{z} = \frac{\bar{z}_{12}\bar{z}_{34}}{\bar{z}_{13}\bar{z}_{24}}, \quad (9)$$

with $z_i \equiv z(w_i)$, $z_{ij} = z_i - z_j$ and similarly for \bar{z} . From the conformal map, we can also show that $z_3 = -z_1$ and $z_4 = -z_2$ (similarly for \bar{z}).

Once we plug the insertion points of the operators (2), in the $\epsilon \rightarrow 0$ limit, the cross-ratios become periodic functions of time, as shown on Fig. 2. The difference with the CFT on the infinite line is that in one cycle of time equal to N , both z and \bar{z} reach their maximal value of 1. More precisely, $z \sim 1$ in the time $[t_i, t_o] = [l + \alpha N, l + L + \alpha N]$ and zero outside, whereas $\bar{z} \sim 1$ inside $[\bar{t}_i, \bar{t}_o] = [N - (l + L) + \alpha N, N - l + \alpha N]$ and zero outside, for integer period α . In order to extract the increase in the second Rényi entropy analytically in the $\epsilon \rightarrow 0$ limit, we simply take the limit of $(z, \bar{z}) \rightarrow (1, 0)$ or $(z, \bar{z}) \rightarrow (0, 1)$ in (8) in the appropriate time intervals.

Let us focus on the explicit example of the Ising model. For the σ operator, from the fusion rule $\sigma \times \sigma = 1 + \varepsilon$, the correlator can be decomposed as [1]

$$\mathcal{G}_{\sigma\sigma}^{\sigma\sigma}(z, \bar{z}) = (C_{\sigma\sigma}^1)^2 |\mathcal{F}_{\sigma\sigma}^{\sigma\sigma}(1|z)|^2 + (C_{\sigma\sigma}^\varepsilon)^2 |\mathcal{F}_{\sigma\sigma}^{\sigma\sigma}(\varepsilon|z)|^2, \quad (10)$$

with the three-point coefficients $C_{\sigma\sigma}^1 = 1$ and $C_{\sigma\sigma}^\varepsilon = \frac{1}{2}$, as well as the conformal blocks

$$\mathcal{F}_{\sigma\sigma}^{\sigma\sigma}(1|z) = \frac{1}{\sqrt{2}} \frac{\sqrt{1 + \sqrt{1 - z}}}{(z(1 - z))^{\frac{1}{8}}}, \quad \mathcal{F}_{\sigma\sigma}^{\sigma\sigma}(\varepsilon|z) = \sqrt{2} \frac{\sqrt{1 - \sqrt{1 - z}}}{(z(1 - z))^{\frac{1}{8}}}. \quad (11)$$

We can then check that the non-zero contribution in the two time intervals comes from the identity block and is equal to $\Delta S_A^{(n)} = \log \sqrt{2}$, in accordance with the modular S-matrix elements. This behavior is naturally explained from the quasi-particle picture where left and right moving sets of quasi-particles propagate from the insertion point of the operator and, on the circle, there are two time intervals where either left or right particles are inside the entangling interval A .

On the other hand, for the ε excitation, using the fusion $\varepsilon \times \varepsilon = 1$, we can write the correlator as

$$\mathcal{G}_{\varepsilon\varepsilon}^{\varepsilon\varepsilon}(z, \bar{z}) = (C_{\varepsilon\varepsilon}^1)^2 |\mathcal{F}_{\varepsilon\varepsilon}^{\varepsilon\varepsilon}(1|z)|^2, \quad (12)$$

with $C_{\varepsilon\varepsilon}^1 = 1$ and conformal block

$$\mathcal{F}_{\varepsilon\varepsilon}^{\varepsilon\varepsilon}(1|z) = \frac{1 - z + z^2}{z(1 - z)}. \quad (13)$$

Clearly, inserting the cross-ratios and taking $\epsilon \rightarrow 0$ yields $\Delta S_A^{(n)} = 0$ for all times. This suggests that the quasiparticles produced by ε are in a product state.

After this short review, below we perform the numerical analysis and compare how the CFT predictions are reproduced on the discrete chain.

III. SINGLE EXCITATIONS IN ISING SPIN CHAIN

We consider quantum Ising model in a transverse magnetic field on a 1d chain of N spins-1/2 described by the Hamiltonian

$$\hat{H} = - \sum_{n=1}^N [\hat{\sigma}_n^x \hat{\sigma}_{n+1}^x + g \hat{\sigma}_n^z], \quad (14)$$

where $\hat{\sigma}_n^{x,z}$ are the standard Pauli matrices acting on n -th spin and we assume periodic boundary conditions $\vec{\sigma}_1 = \vec{\sigma}_{N+1}$. The model is critical for $g = \pm 1$ and unless stated otherwise, in this article we set $g = 1$.

The model can be mapped onto the free fermion system using the Jordan-Wigner transformation and our numerical results are performed in such a setup. We refer to the Appendix A for details. After the mapping, the Hamiltonian can be diagonalized as [13]

$$\hat{H} = \sum_k \epsilon_k \left(\hat{\gamma}_k^\dagger \hat{\gamma}_k - \frac{1}{2} \right), \quad (15)$$

where $\hat{\gamma}_k$ are the fermionic annihilation operators. The ground state of \hat{H} is the vacuum state annihilated by all $\hat{\gamma}_k$ and the dispersion relation reads

$$\epsilon_k = 2\sqrt{(g - \cos k)^2 + \sin^2 k}, \quad (16)$$

where the quasi-momenta k take discrete values $\in [-\pi, \pi]$.

Even at the critical point, for $g = 1$, the dispersion relation is not strictly linear for all values of $k \in [-\pi, \pi]$ due to the discrete nature of the system, approaching linear behaviour only in the limit of long-wavelength $|k| \ll 1$. As a result, the velocity of the quasiparticles depends on the momentum k , especially for larger values of $|k|$ – in contrast with what is the case for CFT. In order to account for that, as well as for comparisons with CFT, we simultaneously consider the model with linearized dispersion relation fixing the velocity of quasiparticles,

$$\hat{H}_{lin} = \sum_k \epsilon_k^{lin} \left(\hat{\gamma}_k^\dagger \hat{\gamma}_k - \frac{1}{2} \right), \quad (17)$$

where $\epsilon_k^{lin} = v_F |k|$ and $\hat{\gamma}_k$ are the annihilation operators diagonalizing Ising Hamiltonian in Eq. (15). In our conventions, $v_F = 2$ is the velocity of quasiparticles at the critical point for that Hamiltonian in the long-wavelength limit of $k \rightarrow 0$, but we will present our plots appropriately rescaled for comparisons with CFT.

Next, we study the evolution of Rényi entanglement entropies in states locally excited by operators on the lattice. More precisely, we excite the ground state of the critical Ising model with local operators $\mathcal{O}(n)$, which can have support on more than one lattice site, and perform a unitary time evolution. We then numerically calculate the entropy of a block A of L consecutive spins at a distance l from the excitation for different times and subtract from it the entropy of the block with no excitation. This setup is schematically illustrated in Fig. 1.

The lattice operators that have σ and ϵ fields as their leading contributions in the continuum are [14]

$$\sigma(n) = \hat{\sigma}_n^x, \quad (18)$$

$$\varepsilon(n) = \hat{\sigma}_n^x \hat{\sigma}_{n+1}^x - \hat{\sigma}_n^z. \quad (19)$$

Moreover, to confront the CFT predictions for other members of a given conformal family, we also consider the simplest descendant, namely the spatial discrete derivative of the σ field

$$d\sigma(n) = \hat{\sigma}_{n+1}^x - \hat{\sigma}_n^x. \quad (20)$$

that corresponds to descendant $\partial_x \sigma(z, \bar{z})$.

In the following sections, we discuss the results for classes of states locally excited by these three different operators.

A. $\sigma(n)$ excitation

The results for $\sigma(n)$ excitation are collected in Fig. 3. Column (a) shows the change in entropy for fixed L and l . We observe the expected plateau appearing at a time when $t \cdot v_F \simeq l$ – and subsequent plateaus when the signal enters the block A from the opposite side or after making some number of circle around the chain. The plateau is however oscillating slightly and then vanishing in a long tail for $t \cdot v_F > l + L$. The mean values in the first plateau are $\Delta S_A^{(2)} \approx 0.51 \log 2$ and $\Delta S_A^{(1)} \approx 0.54 \log 2$, close to the expected value of $\log \sqrt{2}$. Both the oscillations and the tail visible for the first plateau are mostly independent of the system size. When we use linearized Ising Hamiltonian \hat{H}_{lin} (dashed lines) in place of Ising Hamiltonian \hat{H} (solid lines) both the oscillations and the tails disappear and fully periodic structure consistent with the CFT prediction is recovered. This supports the natural interpretation that the tail is related to different velocities of excited quasiparticles which naturally appear for local Hamiltonian on a chain and in this case are smaller than v_F . Notice also that the dashed line has smooth edges, what can be interpreted as manifestation of the nonzero ϵ on the lattice, compare with Fig. 2. Finally, for \hat{H} , the subsequent plateaus appearing for longer times are visibly shifted up, as the signal is slowly dissipating.

Column (b) shows the change of entropy when both l and L are proportional to the system size N and the time is properly rescaled. This validates that the obtained value of ΔS_A is independent of the block size – in contrast to the subtracted background entropy of the block without excitation which in this case grows logarithmically with $L \sim N$. Additionally, we observe that after the rescaling the tails for different $L \sim N$ are collapsing – at least up to corrections which are not visible in this scale and for short enough times – which suggests that the characteristic time scale at which the tails are disappearing is proportional to the block size.

Finally, in column (c) we place the excitation symmetrically with respect to the block, so that the quasiparticle with the same absolute momentum traveling left and right should be entering the block at the same time. Even in this setup ΔS_A acquires large non-zero value when the fastest quasiparticles traveling with v_F reach block A from both sides. This shows that the simplest interpretation valid for global (translationally invariant) quench that only the pairs of quasiparticles with opposite momenta $\pm k$ contribute to the entanglement is no longer valid for local excitation which breaks translational invariance. This signal almost disappears when \hat{H}_{lin} is used and all the quasiparticles enter or leave the block in the same instance of time. We refer for a consistent discussion in the context of local quenches to [15] and evolution of the negativity to [16].

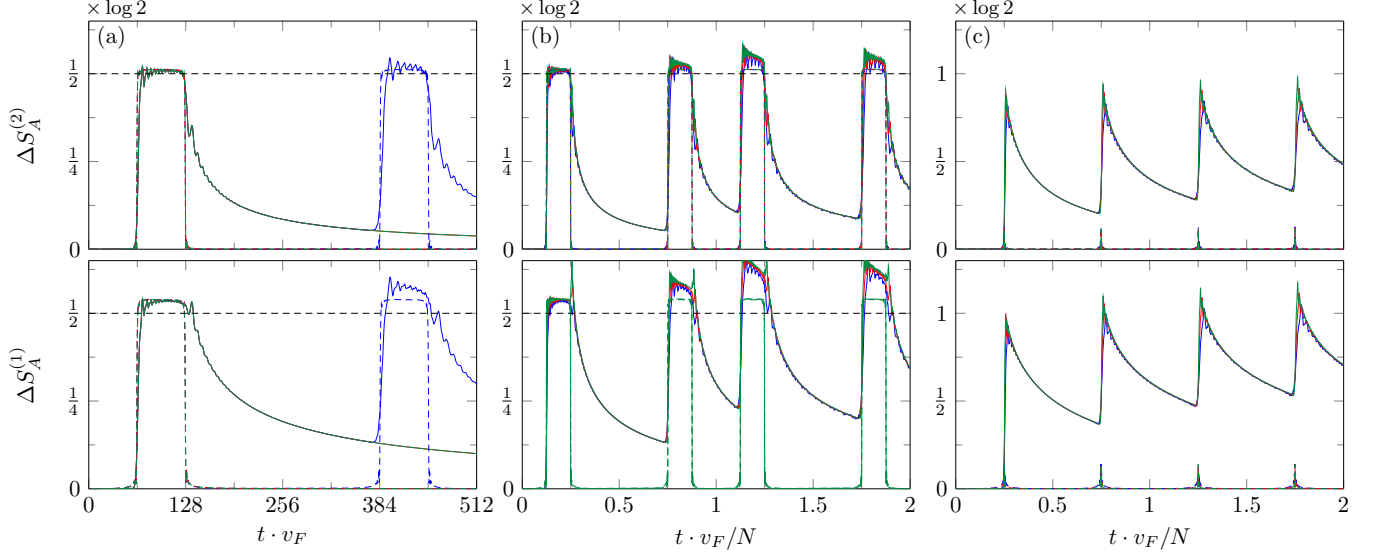


FIG. 3. Evolution after excitation by $\sigma(n)$. Results for Ising Hamiltonian (solid lines) and linearized Ising Hamiltonian (dashed lines). Different system sizes $N = 512$ (blue), $N = 1024$ (red) and $N = 2048$ (green). (a) Fixed block size $L = 64$ and distance $l = 64$. (b) Distance and block size as a fraction of the system size, $L = l = N/8$. (c) Excitation in the same distance from both ends of the block; Block size as a fraction of the system size $L = N/2 + 1$, $l = N/4$. See text for discussion.

B. $\varepsilon(n)$ excitation

The results for $\varepsilon(n)$ excitation are presented in Fig. 4. For fixed l and L in column (a) we obtain non-zero signal with sharp peaks when the signal is first entering and leaving the block, which then disappears in a long tail. When the evolution is governed by \hat{H}_{lin} the tails are not present and we recover the periodic structure of plateaus, which however acquire non-zero values of $\Delta S_A^{(2)} \approx 0.28 \log 2$, and $\Delta S_A^{(1)} \approx 0.56 \log 2$. Interestingly, in this case, there are still

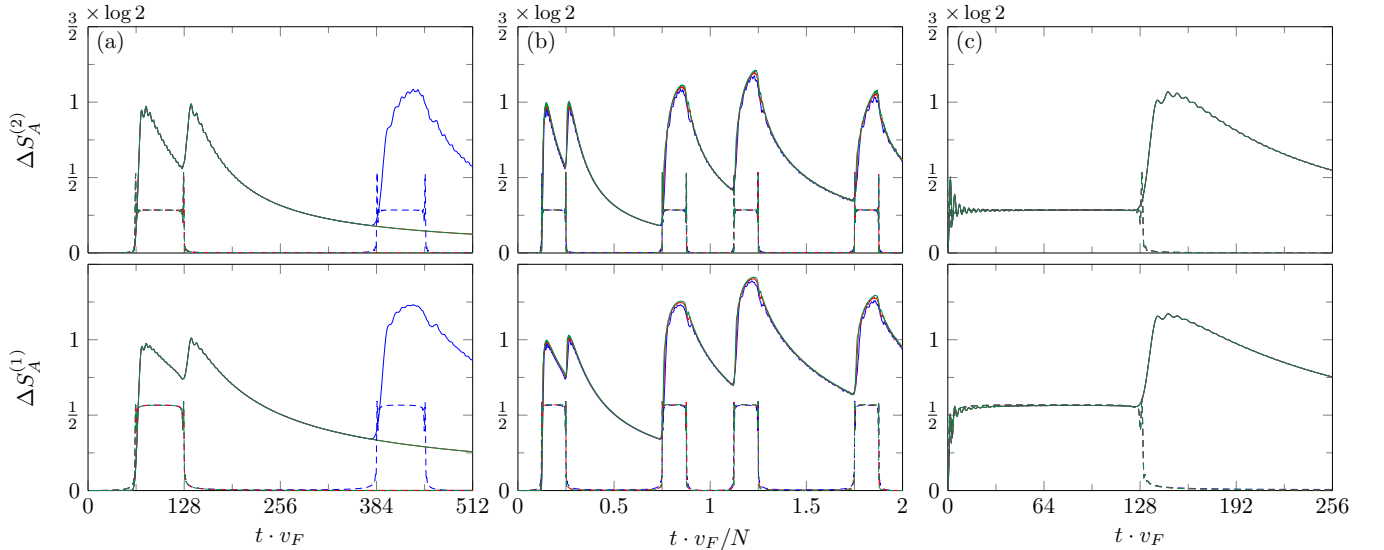


FIG. 4. Evolution after excitation by $\varepsilon(n)$. Results for Ising Hamiltonian (solid lines) and linearized Ising Hamiltonian (dashed lines). System sizes $N = 512$ (blue), $N = 1024$ (red) and $N = 2048$ (green). (a) Fixed block size $L = 64$ and distance from the block $l = 64$; (b) Block size and distance as a fraction of the system size, $L = l = N/8$. (c) Block next to the excitation with $l = 1$ and the block size $L = 128$. See text for discussion.

additional sharp peaks when the signal is entering or leaving the block, which are similar to the structure obtained from CFT with small but finite ϵ . We are however not able to explain the value of ΔS_A in the plateaus as the logarithm of the quantum dimension of ε that should be zero. We conclude that the sub-leading contributions to $\varepsilon(n)$ in the continuum turn out to be more relevant than for $\sigma(n)$. At the same time the observed results suggest that the quasiparticles with large k significantly contribute to the observed value of entanglement, which might be related here with the fact that $\varepsilon(n)$ is supported on two lattice sites.

The stability of the obtained signal is validated in column (b) where we set L and l proportional to system size N , and after properly rescaling of the time we observe the collapse of ΔS_A for different values of N .

Finally, in (c) we show that the non-zero value of ΔS_A obtained in the plateaus for \hat{H}_{lin} can be also recovered from the evolution governed by the original Ising Hamiltonian \hat{H} when the block A is placed just next to excitation. This way difference in velocity of excited quasiparticles turn out to be unimportant for the first plateau as (almost) all right-moving quasiparticles are able to enter the block and the situation resembles that for \hat{H}_{lin} . This suggests that similar strategy can be used in general spin chains, which cannot be mapped onto system of free fermions which we use to construct \hat{H}_{lin} . Such systems can be conveniently simulated using the toolbox of matrix product states (MPS) [17], where, for instance, specific algorithms to study the dynamics of localized excitations in infinite systems have been put forward [18].

C. $\sigma(n+1) - \sigma(n)$ excitation

The results for the discrete spatial derivative of $\sigma(n)$ are collected in Fig. 5. We note that, on the contrary to the two previous cases, the operator $d\sigma(n) = \sigma(n+1) - \sigma(n)$ is not unitary, so even at $t = 0$ it changes the entropy of a block supported on sites other than n and $n+1$. We however see that this effect is relatively small and vanishing with increasing l .

In column (a), for fixed l and L , we observe that ΔS_A does not form plateaus and then disappears in a long tails, which suggests that the slower quasiparticles with large k significantly contribute to the observed signal. This is further corroborated by using \hat{H}_{lin} which allows to recover the periodic structure of plateaus with the values at the peaks close to $\frac{3}{2} \log 2$ predicted by CFT. Similar observation also hold in column (b) for l and L proportional to the system size N .

Finally, in column (c), similarly to the situation in the previous section, we observe that for local Ising Hamiltonian \hat{H} we are able to recover the structure of the first plateau with the peak value $\simeq 1.5 \log 2$ if the block A is placed just next to the excitation and $l = 1$.

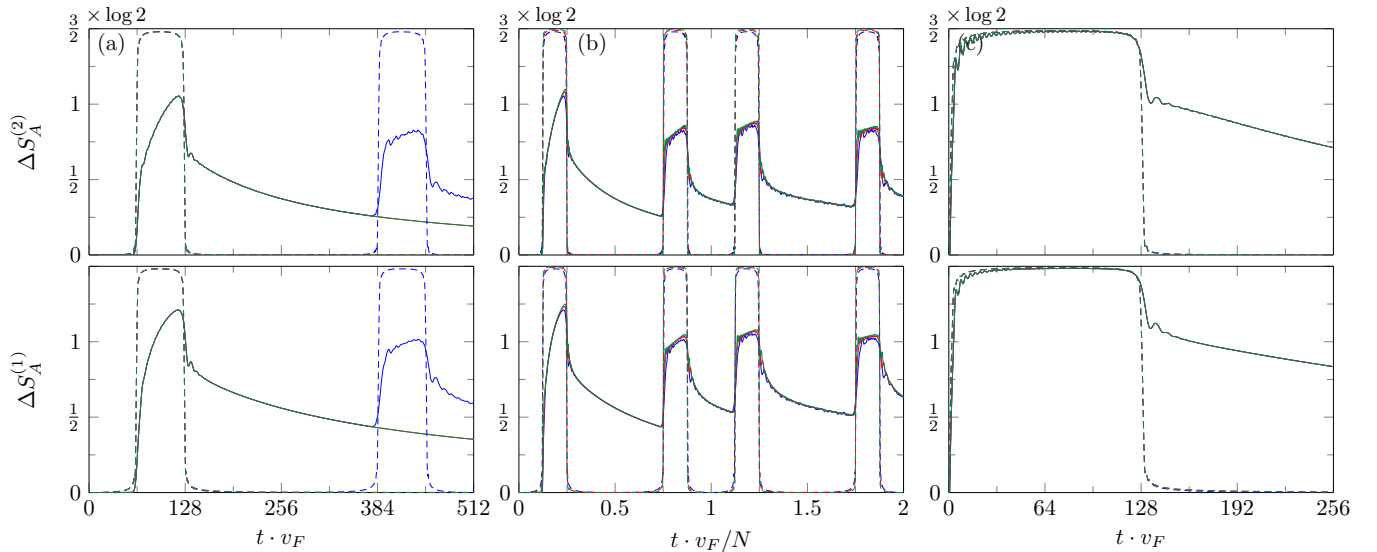


FIG. 5. Evolution after excitation by $\sigma(n+1) - \sigma(n)$. Results for Ising Hamiltonian (solid lines) and linearized Ising Hamiltonian (dashed lines). System sizes $N = 512$ (blue), $N = 1024$ (red) and $N = 2048$ (green). (a) Fixed block size $L = 64$ and distance from the block $l = 64$; (b) Block size and distance as a fraction of the system size, $L = l = N/8$. (c) Block next to the excitation with $l = 1$ and the block size $L = 128$. See text for discussion.

IV. NON-CRITICAL EVOLUTION AND GENERAL EXCITATIONS

In this section we present numerical results that, in principle, could be reproduced from CFT, but in practice the analytical computations become very difficult. In such cases numerics is a great tool for understanding the phenomenology of entanglement evolution and we explore it below. Since we successfully recovered the CFT predictions for the spin σ operator, we will mostly consider states excited by applying σ^x to the lattice sites, but we believe that the universal features of our analysis remain valid for other conformal families.

We begin with evolution of entanglement of a block of spins after exciting the ground state by local operator but in the non-critical model. Having the diagonalized Ising Hamiltonian for any value of the parameters, we can study the evolution of the Rényi entropies away from the critical point. In Fig. 6 we plot the evolution of the second Rényi entropy after acting with $\sigma(n)$ for a few values of g around the critical one.

Clearly, in each case the entropy only changes after time of order l , however the clear plateau with the logarithm of the quantum dimension only appears at criticality. This, in principle, might serve as a proxy for seeing the critical point with local excitations but in general the value of the plateau might be a more complicated expression in terms of the quantum dimensions of the model.

Figure 6 also indicates that the critical Hamiltonian leads to the smallest increase of entanglement of the block after we excite a vacuum by a local operator. Based on our limited analysis, it is not obvious if this lower bound is universal and satisfied by general families of Hamiltonians that have a critical point in their parameter space. It would be very interesting to provide further checks using other available methods – like e.g. MPS – in order to support this observation or possibly find counter-examples.

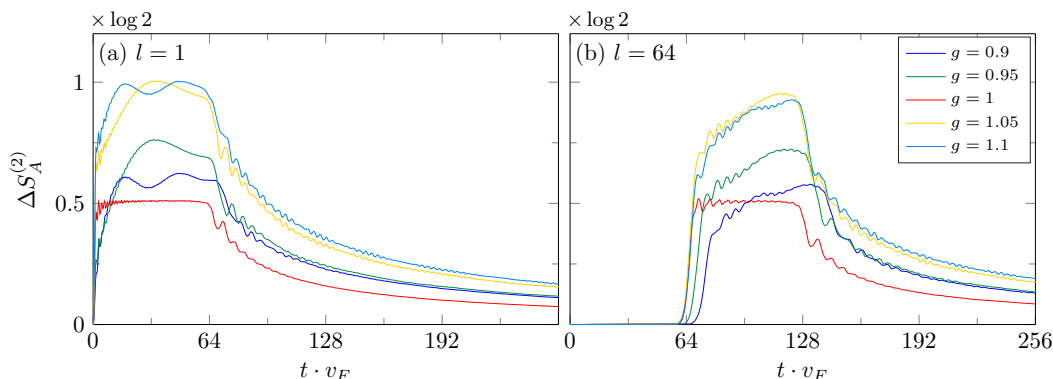


FIG. 6. Evolution of the change in the second Rényi entropy after $\sigma(n)$ excitation for different values of the magnetic field g . The distance of excitation from the block is (a) $l = 1$ and (b) $l = 64$. $L = 64$, $N = 512$.

Next, by using the map to free fermions we can also study more general excited states by acting with multiple local operators on the critical chain. On the other hand, the computations in CFT using the replica trick become very cumbersome and were only done for two excitations in [19]. This part will then serve as a collection of new predictions for the evolution of the Rényi entanglement entropies in (rational) CFTs.

We begin with states where few operators were inserted on sufficiently separated sites and in some distance to the entangling block. We chose the block to be large enough so that there is a time where all the excited quasiparticles are inside the entangling region. From numerical results it is clear that in such excited states the entanglement entropy is a sum of the quantum dimensions of the operators, see Fig. 7 for a case of 3 and 5 σ -excitations. The time evolution of entanglement in such states is very similar to periodic quench studied, e.g., in Ref. [20].

Based on these observations, we conjecture that in rational CFTs, and more generally CFTs for which the quasiparticle picture remains a good effective description of the dynamics of entanglement, for m such excitations the change in maximal contribution to the entanglement Rényi entropies is simply

$$\Delta S_L^{(n)} = \sum_{i=1}^m \log d_i \quad (21)$$

with quantum dimension of the i th operator d_i (can be different or the same). We verify numerically, using \hat{H}_{lin} , that if we use some combination of operators $\sigma(n)$, $\epsilon(n)$ and $d\sigma(n)$ placed in the setup considered in Fig. 7 where

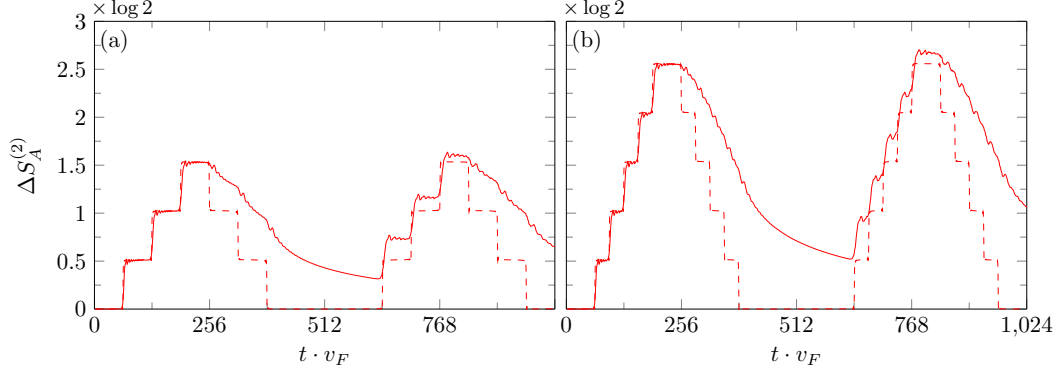


FIG. 7. Evolution after exciting by $\sigma(n)$ on (a) 3 sites, $n \in \{1, 65, 129\}$ and (b) 5 sites, $n \in \{1, 33, 65, 97, 129\}$. Results for Ising Hamiltonian (solid lines) and linearized Ising Hamiltonian (dashed lines). Block A supported on sites $193, \dots, 384$ ($L = 192$). $N = 1024$.

the insertion points are sufficiently separated, then the total increase of the entropy of the block A indeed is a sum of contributions from single excitations discussed in section III. A similar result was reported in free quantum field theories in [5] but it would be very interesting to formulate at least a necessary conditions for the validity of this formula in arbitrary interacting 2d CFT and we leave this as an open future problem.

Another class of excited states that we consider is defined by acting with local operators on all the sites of the chain

$$|\psi_G\rangle = \prod_{i=1}^N \hat{\mathcal{O}}_i |0\rangle. \quad (22)$$

They could be thought of as a version of a global quench [3] and have recently been employed in large c holographic CFTs as states dual to the matter collapsing to a black hole [21].

As we can see, the evolution looks qualitatively similar to the global quench in the finite size system [3], but the final value in that case is given by the entropy density times the length of the interval. Here, the evolution of entanglement entropies can still be interpreted in terms of the quasiparticles propagating from the lattice sites to the left and right. This picture suggests that the maximal value of the entropies is equal to $\Delta S_{max}^{(n)} = 2L \log d_O$, where the factor of two comes from the fact that at each site we can have two (left and right) quasiparticles. On the other hand, the maximal value of the entropy of the block of L spins is attained by the density matrix with all 2^L eigenvalues equal and is also equal to $L \log 2$. Apparently these two numbers coincide for $d_\sigma = \sqrt{2}$ and the value of the plateaux for $\Delta S^{(2)}$ is equal to this maximal value minus the ground state entropy, i.e. $S^{(2)}$ attains its maximal possible value, which can be seen in Fig. 8 for \hat{H}_{lin} . If Ising Hamiltonian \hat{H} is used instead, the maximal value of the plateaux is not reached

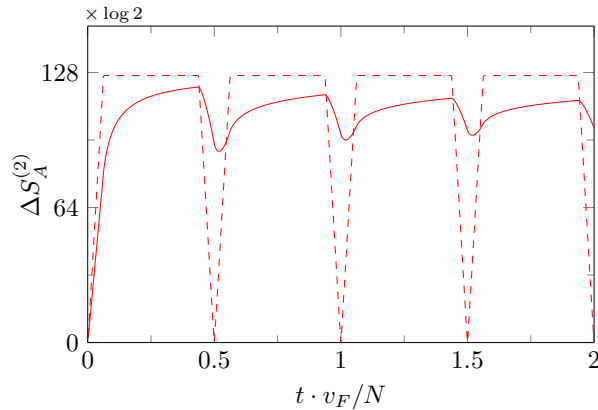


FIG. 8. Evolution after exciting all the sites by σ^x . Block size $L = 128$ and the system size $N = 1024$.

and the clean periodic structure of revivals is obscured, showing the relevance of coherent dynamics of quasiparticles for obtaining those effects. In other words, the memory effects for the quasiparticles in the critical model seem to be suppressed by entanglement between quasiparticles with different momenta and for late times entanglement measures saturate.

It would be interesting to compare how this behaviour changes for local operators with different quantum dimensions and for different densities of excitations leading possibly to a saturation, so we leave it as another open problem. Moreover, according to [21], in the large c CFTs, entanglement entropy saturates at the thermal value with an effective temperature and the time for returning into the initial value (Poincare recurrence) is expected to be exponential in the central charge. It would be also interesting to further explore what happens in between these two regimes and how our memory effects are corrected once we consider states in chaotic or non-local toy models for black holes as for instance in Ref. [22, 23].

V. RELATIVE ENTROPY

We finish our numerical explorations with evolution of the relative entropy at criticality. As far as we are aware, numerical analysis of the relative entropy in critical systems has been much less explored than the Rényi entropies. Nevertheless, it is an important tool for understanding the notion of the distance between quantum states in field theories and plays an interesting role in uncovering the features of holographic CFTs [24]. The relative entropy is defined for two reduced density matrices $\hat{\rho}$ and $\hat{\vartheta}$ as

$$S(\rho|\vartheta) = \text{Tr}(\hat{\rho} \log \hat{\rho}) - \text{Tr}(\hat{\rho} \log \hat{\vartheta}). \quad (23)$$

In general excited state of a 2d CFT, the second term makes it very hard to compute analytically. Even for locally excited states the replica method requires the knowledge of the correlation function of $2n$ operators in order to continue to $n \rightarrow 1$, see, e.g., [12, 25]. On the other hand, if we compare excited states $\hat{\rho}$ with $\hat{\vartheta}$ obtained in the vacuum, given that the reduced density matrix $\hat{\vartheta}$ can be written as the exponent of a known modular Hamiltonian, $\hat{\vartheta} = e^{-\hat{H}_m} / \text{Tr}(e^{-\hat{H}_m})$, we can express the entropy as

$$S(\rho|\vartheta) = \Delta\langle\hat{H}_m\rangle - \Delta S^{(1)}. \quad (24)$$

The expectation value of the vacuum modular Hamiltonian $\Delta\langle\hat{H}_m\rangle = \text{Tr}(\hat{\rho}\hat{H}_m) - \text{Tr}(\hat{\vartheta}\hat{H}_m)$ is computed in the excited state and $\Delta S^{(1)}$ denotes the difference of the von-Neumann entropies of the two density matrices, see [26] for more details.

Now, in 2d CFTs, the expectation value of the vacuum modular Hamiltonian for an interval of length L in a state locally excited by a primary operator is universal. Namely, it follows from the OPE of the stress tensor with the primary operator, and can be computed from (see e.g. [27])

$$\Delta\langle\hat{H}_m\rangle = \frac{\pi}{L} \int_L dx (L-x)x \langle T_{00}(x) \rangle. \quad (25)$$

Moreover, as we argued in section II, the change of the entanglement entropy of the block is equal to the logarithm of the quantum dimension of the primary operator. From these two results we evaluate the relative entropy in our CFT setup and we can possibly compare it with numerics.

In the following, we simply take $\hat{\vartheta}$ to be the reduced density matrix of a block of L spins in the ground state and $\hat{\rho}$ as the density matrix (1) of the block for the state locally excited by operator $\sigma(n)$ in a distance l from the block. We find an elegant expression for the relative entropy in terms of fermionic covariance matrices for Gaussian $\hat{\rho}$ and $\hat{\vartheta}$

$$S(\rho|\vartheta) = \text{Tr}(C_L^\rho \log C_L^\rho) - \text{Tr}(C_L^\rho \log C_L^\vartheta), \quad (26)$$

and we refer to the Appendix A for details. We only notice here that as C_L^ρ and C_L^ϑ , or equivalently $\hat{\rho}$ and $\hat{\vartheta}$, cannot be simultaneously diagonalized, finite numerical precision limits the calculation of the second term in the above expression only to relatively small block sizes. We present the results in Fig. 9.

We observe that the signal strongly changes depending if \hat{H} or \hat{H}_{lin} is governing the time evolution. For the Ising Hamiltonian \hat{H} the maximum of the relative entropy for given block size L quickly disappears with the distance between the block and the excitation – suggesting that modes with high momenta contribute significantly to the observed value. If linearized Ising Hamiltonian \hat{H}_{lin} is used instead, the signal does not dissipate, with both the width and the value at the peak being proportional to L .

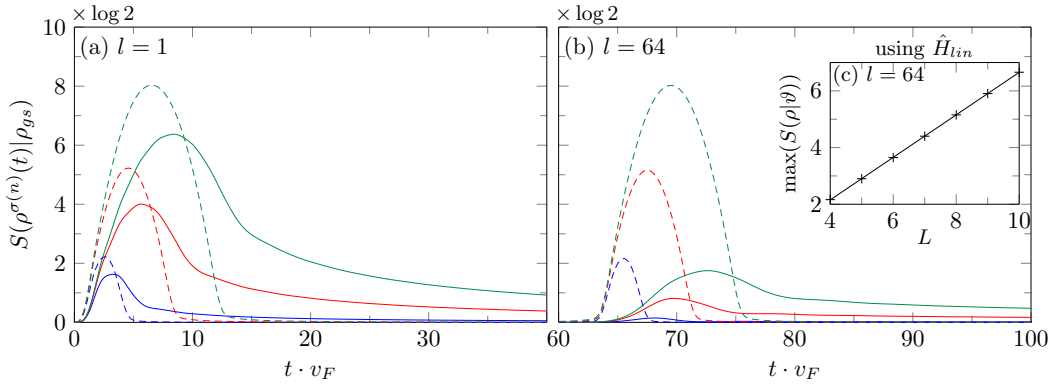


FIG. 9. Evolution of Relative Entropy after excitation by $\sigma(n)$. Colors indicate different block sizes $L = 4$ (blue), $L = 8$ (red), $L = 12$ (green). Results for Ising Hamiltonian (solid lines) and linearized Ising Hamiltonian (dashed lines). Distance of the entangling block from the excitation (a) $l = 1$, (b) $l = 64$. $N = 1024$. Inset (c) shows the maximum of relative entropy from panel (b) for linearized Ising Hamiltonian, where the linear fit $\simeq 0.75L - 0.85$.

One can verify that, for non-zero ϵ , the numerical evolution of the relative entropy is consistent with the CFT computation with the expectation value of the stress tensor in our locally excited state. Moreover, it is possible to compute in CFT the value of the peak of the relative entropy. The maximum of the relative entropy is universal in the small ϵ limit

$$\max(S(\rho|\vartheta)) \simeq E_{\mathcal{O}}L + O(\epsilon), \quad (27)$$

where the energy due to the operator insertion is $E_{\mathcal{O}} \sim \Delta_{\mathcal{O}}/\epsilon$. Numerically, this is shown on the inset in Fig. 9 where we see the linear growth of the peak of the relative entropy with the length of the interval. Our numerical results in the Ising chain are consistent with the energy $E_{\sigma(n)} = \langle \Psi^{\sigma(n)}(t) | \hat{H}_{lin}/v_F | \Psi^{\sigma(n)}(t) \rangle - \langle 0 | \hat{H}_{lin}/v_F | 0 \rangle \simeq 0.742$ close to the slope $\simeq 0.75$ fitted in Fig. 9(c).

Let us finally compare our formula (27) with the first-law for entanglement entropy for a family of the nearby equilibrium states [26, 29] that reads $\Delta E \sim T_e \Delta S$ with $T_e \sim L^{-1}$. This relation is a consequence of the vanishing relative entropy. Interestingly, we observe an analogous first-law like relation for the maximal value of the distance between our two quantum states as measured by the relative entropy. Moreover, the maximal value is universal and contained in $\Delta\langle \hat{H}_m \rangle$. The details of the CFT analysis for this class of locally excited states will appear elsewhere [28].

VI. DISCUSSION

We have shown that, by using local operators on the critical lattice, one is able to extract further non-trivial CFT data – like quantum dimensions – numerically. We have successfully done so for the spin operator σ and its derivative descendant. However, we also saw that, even after linearization of the dispersion relation, the lattice energy operator gave a non-zero contribution to the entropy of a block. This fact might be explained by the ambiguity in the identification between the lattice and the CFT operators or a non-trivial contribution from the “tail” of operators in the continuum and deserves further investigation.

Our analysis could be naturally extended to other CFTs with operators that enjoy known lattice counterparts. A natural setup might be the three-state Potts model in which [11] recently analyzed the lattice realization of the local operators in the parafermionic CFT. Clearly, it would be much more interesting to explore analytically what is the contribution from a general lattice operator and what kind of information can be extracted from the increase in Rényi entropies. In fact there has been a lot of work on extracting local CFT operators from the multiscale entanglement renormalization ansatz (MERA) [30]. It would be interesting to apply those developments in the studies of entanglement evolution after local operator excitations.

The evolution of entanglement measures after local excitations away from the critical point appears to be relatively unexplored. As we saw, the critical behavior appears to be very special – characterized by formation of a clear plateau – and might be used as a smoking gun of a critical point. Moreover, the contribution to the Rényi entropies appears to be the smallest for the Ising Hamiltonian with critical parameters what might be a sign of a general bound. We hope that our analysis will serve as a starting point for more complicated systems and will help to uncover other unknown universal phenomena in the propagation of entanglement.

Last but not least, we performed the evolution of the relative entropy between the vacuum and a locally excited state. Interestingly, this distance measure shows universal features analogous to the first law of entanglement and its maximum – maximal quantum distance – is proportional to the change in the energy with an effective temperature. Exploring this relation in CFTs or free field theories where explicit computations are under control opens a new interesting path for investigation.

Acknowledgements We would like to thank John Cardy, Paul Fendley, Masahiro Nozaki, Tokiro Numasawa, Tadashi Takayanagi, Kento Watanabe, Luca Tagliacozzo and Alvaro Veliz-Orsorio for correspondence and discussions. We would also like to thank Xueda Wen for comments sharing some of his unpublished results. We acknowledge support by the Swedish Research Council (VR) grant 2013-4329 (P.C.) and Narodowe Centrum Nauki (NCN, National Science Center) under Project No. 2013/09/B/ST3/01603 (M.M.R.). P.C. would like to thank Yukawa Institute for Theoretical Physics for hospitality and support during the "Quantum Information in String Theory and Many-body Systems" workshop where some of this work was performed. We would like to thank the organizers of the Tensor Network Summer School in Ghent where this work was initiated.

Appendix A: Details of simulations

Hamiltonian.— The Ising Hamiltonian (14) is diagonalized in a standard way [31] by mapping it onto a system of free fermions using the Jordan-Wigner transformation

$$\begin{aligned}\hat{\sigma}_n^z &= 1 - 2\hat{c}_n^\dagger \hat{c}_n, \\ \hat{\sigma}_n^x + i\hat{\sigma}_n^y &= 2\hat{c}_n \prod_{m<n} (1 - 2\hat{c}_m^\dagger \hat{c}_m),\end{aligned}\tag{A1}$$

where \hat{c}_n are fermionic annihilation operators. For convenience, we introduce Majorana fermions $\hat{a}_{2n-1} = \hat{c}_n + \hat{c}_n^\dagger$, $\hat{a}_{2n} = i(\hat{c}_n - \hat{c}_n^\dagger)$ which are hermitian, unitary and satisfy canonical anticommutation relations $[\hat{a}_m, \hat{a}_n]_+ = 2\delta_{m,n}$. The Ising Hamiltonian with periodic boundary conditions can be rewritten as

$$\hat{H} = \hat{H}^+ \hat{P}^+ + \hat{H}^- \hat{P}^-.\tag{A2}$$

Above, $\hat{P}^\pm = \frac{1}{2}(1 \pm \hat{P})$ are projectors on the subspaces with respectively even and odd number of fermions, where the parity operator $\hat{P} = \prod_{n=1}^N \hat{\sigma}_n^z = e^{i\pi \sum_n \hat{c}_n^\dagger \hat{c}_n}$ commutes with \hat{H} . The Hamiltonians in both subspaces can be expressed in terms of fermionic operators as

$$\hat{H}^\pm = - \sum_{n=1}^N \left(\frac{i}{2} \hat{a}_{2n} \hat{a}_{2n+1} + \frac{ig}{2} \hat{a}_{2n-1} \hat{a}_{2n} + h.c. \right),\tag{A3}$$

differing only at the boundary term. This is accounted for by enforcing the boundary conditions: antiperiodic $\hat{a}_{2N+n} = -\hat{a}_n$ for \hat{H}^+ , and periodic $\hat{a}_{2N+n} = \hat{a}_n$ for \hat{H}^- . For $g > 0$, which we use in this work, the ground state of \hat{H} belongs to the subspace with even parity for any value of N , see e.g. Ref. [32].

It is convenient to introduce $\hat{H}^\pm = \vec{\hat{a}}^\dagger \mathbf{H}^\pm \vec{\hat{a}}$, where $\vec{\hat{a}}$ is a column vector composed of operators \hat{a}_n and \mathbf{H}^\pm are $2N \times 2N$ hermitian matrices. In the following, we employ the matrix notation whenever it serves to simplify the notation. In each parity subspace the system is solved independently by a canonical transformation to a new base of Majorana fermions, $\vec{\hat{a}} = \mathbf{U}^\pm \vec{\hat{d}}^\pm$, where \mathbf{U}^\pm are real and orthogonal matrices. The Hamiltonian then reads

$$\hat{H}^\pm = \sum_{k_n \in k^\pm} \epsilon_{k_n}^\pm \left(\hat{\gamma}_{k_n}^{\pm\dagger} \hat{\gamma}_{k_n}^\pm - \frac{1}{2} \right),\tag{A4}$$

expressed above in terms of standard annihilation operators $\hat{\gamma}_{k_n}^\pm = (\hat{d}_{2n-1}^\pm - i\hat{d}_{2n}^\pm)/2$. This can be done analytically by a subsequent Fourier and Bogoliubov transformations [31], resulting in ϵ_k given by Eq. (16). The fermionic modes are indexed by quasi-momenta consistent with the respective boundary conditions, i.e. $k_n \in k^+ = \{\pm \frac{\pi}{N}, \pm \frac{3\pi}{N}, \pm \frac{5\pi}{N}, \dots\} \subset [-\pi, \pi]$ for H^+ , and $k_n \in k^- = \{0, \pm \frac{2\pi}{N}, \pm \frac{4\pi}{N}, \dots\} \subset [-\pi, \pi]$ for H^- . This procedure is equivalent to bringing H^\pm into the canonical form $\mathbf{U}^{\pm\dagger} \mathbf{H}^\pm \mathbf{U}^\pm = \bigoplus_{k_n \in k^\pm} \begin{pmatrix} 0 & -i\epsilon_{k_n}/2 \\ i\epsilon_{k_n}/2 & 0 \end{pmatrix}$. We can now formally introduce the linearized Ising

Hamiltonian by H_{lin}^\pm defined as $U^{\pm\dagger} H_{lin}^\pm U^\pm = \bigoplus_{k_n \in k^\pm} \begin{pmatrix} 0 & -i\epsilon_{k_n}^{lin}/2 \\ i\epsilon_{k_n}^{lin}/2 & 0 \end{pmatrix}$, where the linearized dispersion relation $\epsilon_k^{lin} = v_F |k| = 2|k|$.

The ground state of the system, $|0\rangle$, which is the starting point for our further considerations, is the even parity state annihilated by all annihilation operators diagonalizing \hat{H}^+ , namely $\hat{\gamma}_{k_n}^+ |0\rangle = 0$. All the information about this state is encoded in the matrix U^+ .

Local operators and time evolution.— We consider local operators which in the fermionic language read

$$\begin{aligned} \sigma(n) &= \hat{\sigma}_n^x = \prod_{m=1}^{2n-1} \hat{a}_m, \\ \varepsilon(n) &= \hat{\sigma}_n^x \hat{\sigma}_{n+1}^x - \sigma_n^z = \hat{a}_{2n} (\hat{a}_{2n-1} + \hat{a}_{2n+1}), \\ d\sigma(n) &= \hat{\sigma}_{n+1}^x - \hat{\sigma}_n^x = \left(\prod_{m=1}^{2n} \hat{a}_m \right) (i\hat{a}_{2n+1} - \hat{a}_{2n}), \end{aligned} \quad (\text{A5})$$

up to the irrelevant phase factors. We simulate the action of those operators on the ground state by employing the Heisenberg picture. As all operators in Eq. (A5) are expressed as a product of linear combinations of operators \hat{a}_n , this can be done iteratively.

Starting with the simplest case of operator $\hat{O}_1 = \hat{a}_{m_1}$, which is unitary by construction, we define the operator in the Heisenberg picture as

$$\hat{a}_n^{O_1} = \hat{O}_1^\dagger \hat{a}_n \hat{O}_1 = -(-1)^{\delta_{nm_1}} \hat{a}_n = - \sum_j (-1)^{\delta_{nm_1}} [U^+]_{nj} \hat{d}_j^+, \quad (\text{A6})$$

where a new matrix $[U^{O_1}]_{nj} = -(-1)^{\delta_{nm_1}} [U^+]_{nj}$ describes the transformation to the fermionic base in which the initial state is the vacuum – note that operator \hat{O}_1 is applied to the ground state of the Ising Hamiltonian \hat{H}^+ in Eq. (A4). Subsequent application of unitary operators \hat{O}_l for $l = 2, 3, \dots$ is obtained similarly as $\hat{a}_n^{O_l} = \hat{O}_l^\dagger \hat{a}_n^{O_{l-1}} \hat{O}_l$, and $[U^{O_l}]_{nj} = -(-1)^{\delta_{nm_l}} [U^{O_{l-1}}]_{nj}$ for $\hat{O}_l = \hat{a}_{m_l}$, corresponding to the action of the operator $\hat{O} = \hat{O}_l \hat{O}_{l-1} \dots \hat{O}_1$ on the initial ground state.

In a general case when $\hat{O}_1 = \vec{v} \vec{\hat{a}}$, with \vec{v} being a row vector of coefficients, we have to generalize the above procedure. Notice that \hat{O}_1 , in principle, does not have to be unitary. As we are only interested in the action of \hat{O}_1 on the ground state, $|0\rangle$, we introduce unitary operator \hat{Q}_1 , such that $\hat{Q}_1 |0\rangle \sim \hat{O}_1 |0\rangle$ up to normalization. For \hat{Q}_1 to be unitary, it is enough to require that $\hat{Q}_1 = \frac{\vec{w}}{\|\vec{w}\|} \vec{\hat{d}}^+$, where \vec{w} is a row vector of real coefficients. We can now define the operators in the Heisenberg picture

$$\vec{\hat{a}}^{O_1} = \hat{Q}_1^\dagger \vec{\hat{a}} \hat{Q}_1 = U^+ \left(\hat{Q}_1^\dagger \vec{\hat{d}}^+ \hat{Q}_1 \right) = U^+ \left(2 \frac{\vec{w}^\dagger \vec{w}}{\|\vec{w}\|^2} - \mathbb{1} \right) \vec{\hat{d}}^+, \quad (\text{A7})$$

defining new transformation matrix $U^{O_1} = U^+ \left(2 \frac{\vec{w}^\dagger \vec{w}}{\|\vec{w}\|^2} - \mathbb{1} \right)$. The vector \vec{w} is found as $w_{2n-1} = \text{Re}([\vec{v}U^+]_{2n-1} - i[\vec{v}U^+]_{2n})$ and $w_{2n} = -\text{Im}([\vec{v}U^+]_{2n-1} - i[\vec{v}U^+]_{2n})$. This follows from the condition $\hat{O}_1 |0\rangle = \vec{v} U^+ \vec{\hat{d}}^+ |0\rangle = \vec{w} \vec{\hat{d}}^+ |0\rangle = \|\vec{w}\| \hat{Q}_1 |0\rangle$, where the two operators may differ by operators γ_n^+ annihilating the vacuum state $|0\rangle$.

Finally the time evolution is simulated in the Heisenberg picture as $\frac{\partial}{\partial t} \hat{a}_n^O(t) = i[\hat{H}^O(t), \hat{a}_n^O(t)]$, which leads to $\vec{\hat{a}}^O(t) = U(t) \vec{\hat{d}}^+$, where $U(t) = e^{-4iHt} U^O$, and the matrix $H = H^+(H^-)$ for the even (odd) parity of the excited state $\hat{O}|0\rangle$. Notice that operator $\varepsilon(n)$ is preserving the parity, and $\sigma(n), d\sigma(n)$ are changing it. Finally, the time evolution with the linearized Hamiltonian is obtained by using matrices H_{lin}^\pm instead of H^\pm above.

Calculating entropies.— The entropy of a block of consecutive spins is calculated in a standard way [33], as all the information about the reduced density matrix of a block is encoded in the $2L \times 2L$ covariance matrix

$$C_L = \left[\frac{1}{2} \langle 0 | \hat{a}_m(t) \hat{a}_n(t) | 0 \rangle \right]_{m,n=2L_0+1, 2L_0+2, \dots, 2L_0+2L} \quad (\text{A8})$$

supported on L consecutive lattice sites $L_0 + 1, \dots, L_0 + L$. It is found as a submatrix of $C = \frac{1}{2} \langle \Psi^O(t) | \vec{\hat{a}} \vec{\hat{a}}^\dagger | \Psi^O(t) \rangle = \frac{1}{2} \langle 0 | \vec{\hat{a}}^O(t) \vec{\hat{a}}^O(t)^\dagger | 0 \rangle = U(t) C_v U(t)^\dagger$, with $C_v = \frac{1}{2} \langle 0 | \vec{\hat{d}} \vec{\hat{d}}^\dagger | 0 \rangle = \bigoplus_{n=1}^N \begin{pmatrix} 1/2 & -i/2 \\ i/2 & 1/2 \end{pmatrix}$ being the correlation matrix in the canonical (vacuum) base.

Rényi entropy of the block is then found as,

$$S_L^{(\alpha)} = \frac{1}{1-\alpha} \sum_{j=1}^L \log [p_j^\alpha + (1-p_j)^\alpha], \quad (\text{A9})$$

where $\{p_1, 1-p_1, p_2, 1-p_2, \dots, p_L, 1-p_L\}$ are the eigenvalues of C_L . For $\alpha = 1$, the von-Neumann entropy reads

$$S_L^{(1)} = - \sum_{j=1}^L [p_j \log p_j + (1-p_j) \log(1-p_j)] = -\text{Tr}(C_L \log C_L), \quad (\text{A10})$$

where the second equation provides the direct expression in term of covariance matrix C_L . Relative entropy can be similarly found similarly as

$$S(\rho|\vartheta) = \text{Tr}(\hat{\rho} \log \hat{\rho}) - \text{Tr}(\hat{\rho} \log \hat{\vartheta}) = \text{Tr}(C_L^\rho \log C_L^\rho) - \text{Tr}(C_L^\rho \log C_L^\vartheta). \quad (\text{A11})$$

As the matrices $C_L^\rho = C_L$ and C_L^ϑ (calculated as the correlation matrix in the ground state) cannot be diagonalized simultaneously, it becomes difficult to numerically calculate the second term in the above equation for large blocks. In that case C_L^ϑ has many eigenvalues approaching 0, falling below numerical precision, which prevents the calculation of the logarithm. For this reason, in Sec. V, we calculate residual entropy only for small enough block where this problem does not yet occur.

Finally, in order to derive the non-standard second term on the r.h.s. of Eq. (A11) we employ the fact that $\hat{\vartheta}$ is Gaussian and can be expressed as $\hat{\vartheta} = \prod_{j=1}^L (q_j \hat{f}_j \hat{f}_j^\dagger + (1-q_j) \hat{f}_j^\dagger \hat{f}_j)$, where the diagonal form in terms of fermionic annihilation (creation) operators \hat{f}_j (\hat{f}_j^\dagger) can be directly obtained from the correlation matrix $C_L^\vartheta = \frac{1}{2} \langle 0 | \vec{\hat{a}}^L \vec{\hat{a}}^{L\dagger} | 0 \rangle$ [33]. We introduce here $\vec{\hat{a}}^L$ as a column vector consisting of Majorana fermions $\hat{a}_{2L_0+1}, \hat{a}_{2L_0+2}, \dots, \hat{a}_{2L_0+2L}$ in the entangling block. Then $\frac{1}{\sqrt{2}} \vec{\hat{a}}^L = U^\vartheta \vec{\hat{f}}$, where $\vec{\hat{f}}$ is a column vector consisting of $\hat{f}_1, \hat{f}_1^\dagger, \hat{f}_2, \dots, \hat{f}_L^\dagger$, and U^ϑ is a unitary matrix diagonalising $C_L^\vartheta = U^\vartheta \left[\bigoplus_{j=1}^L \begin{pmatrix} q_j & 0 \\ 0 & 1-q_j \end{pmatrix} \right] U^{\vartheta\dagger}$. This allows to compute $\text{Tr}(\hat{\rho} \log \hat{\vartheta}) = \sum_{j=1}^L \langle f_j f_j^\dagger \rangle_{\hat{\rho}} \log q_j + \langle f_j^\dagger f_j \rangle_{\hat{\rho}} \log(1-q_j)$. Using matrix notation this equals $\text{Tr} \left(\left[\bigoplus_{j=1}^L \begin{pmatrix} \langle f_j f_j^\dagger \rangle_{\hat{\rho}} & 0 \\ 0 & \langle f_j^\dagger f_j \rangle_{\hat{\rho}} \end{pmatrix} \right] \left[\bigoplus_{j=1}^L \begin{pmatrix} \log q_j & 0 \\ 0 & \log(1-q_j) \end{pmatrix} \right] \right) = \text{Tr} \left(U^{\vartheta\dagger} C_L^\rho U^\vartheta \left[\bigoplus_{j=1}^L \begin{pmatrix} \log q_j & 0 \\ 0 & \log(1-q_j) \end{pmatrix} \right] \right) = \text{Tr}(C_L^\rho \log C_L^\vartheta)$, which gives Eq. (A11).

-
- [1] Di Francesco P, Mathieu P and Senechal D 1997 *Conformal field theory* (Springer)
 - [2] Holzhey C, Larsen F and Wilczek F 1994 Nucl. Phys. B **424** 443
Calabrese P and Cardy J 2004 J. Stat. Mech. **0406** P06002
Calabrese P and Cardy J 2009 J. Phys. A **42** 504005
 - [3] Calabrese P and Cardy J 2016 J. Stat. Mech. 064003
 - [4] Nozaki M, Numasawa T and Takayanagi T 2014 Phys. Rev. Lett. **112** 111602
 - [5] Nozaki M 2014 JHEP **1410** 147
 - [6] Caputa P, Nozaki M and Takayanagi T 2014 PTEP **2014** 093B06
Caputa P, Simon J, Stikonas A and Takayanagi T 2015 JHEP **1501** 102
Asplund C T, Bernamonti A, Galli F and Hartman T 2015 JHEP **1502** 171
Caputa P, Simon J, Stikonas A, Takayanagi T and Watanabe K 2015 JHEP **1508** 011
Shiba N 2014 JHEP **1412** 152
Guo W Z and He S 2015 JHEP **1504** 099
Guo W Z 2015 arXiv:1510.07142
Nozaki M, Numasawa T and Matsuura S 2016 JHEP **1602** 150
Caputa P, Numasawa T and Veliz-Orsorio A 2016 arXiv:1602.06542
Sivaramakrishnan A 2016 arXiv:1604.00965
David J R, Khetrapal S and Kumar S P 2016 arXiv:1605.05987
Caputa P, Nozaki M and Numasawa T 2016 Phys. Rev. D **93** 105032
Nozaki M, and Watanabe N, arXiv:1606.07076
Zhou T, arXiv:1607.08631
 - [7] Alcaraz F C, Berganza M I and Sierra G 2011 Phys. Rev. Lett. **106**, 201601
Berganza M I, Alcaraz F C and Sierra G 2012 J. Stat. Mech. **1201** P01016

- V. Alba, M. Fagotti and P. Calabrese, 2009 J. Stat. Mech. **0910**, P10020
 Palmai T 2014 Phys. Rev. B **90** 161404
 Sheikh-Jabbari M M and Yavartanoo H 2016 arXiv:1605.00341
 Chen B and Wu J Q 2016 arXiv:1605.06753
 Taddia L, Ortolani F and Palmai T 2016 arXiv:1606.02667
 Giusto S, and Russo R, 2014 Phys. Rev. D **90**, no. 6, 066004
- [8] He S, Numasawa T, Takayanagi T and Watanabe K 2014 Phys. Rev. D **90** 041701
 - [9] Caputa P and Veliz-Orsorio A 2015 Phys. Rev. D **92** 065010
 - [10] Chen B, Guo W Z, He S and Wu J Q 2015 JHEP **1510** 173
 - [11] Mong R S K, Clarke D J, Alicea J, Lindner N H and Fendley P 2014 J. Phys. A **47** 452001
 - [12] Lashkari N 2016 Phys. Rev. Lett. **117** 041601
 - [13] See Appendix A for some technical subtleties related with the boundary conditions.
 - [14] Stojevic V, Haegeman J, McCulloch I P, Tagliacozzo L and Verstraete F 2015 Phys. Rev. B **91** 035120
 - [15] Peschel I and Eisler V 2007 J. Stat. Mech. P06005
 - [16] Wen X, Chang P Y and Ryu S 2015 Phys. Rev. B **92** 075109
 - [17] Verstraete F, Murg V, Cirac J I 2008, Adv. Phys. **57** 143
 Schollwöck U 2011 Ann. Phys. **326** 96
 - [18] Zauner V, Ganahl M, Evertz H G, Nishino T 2015 J. Phys.: Condens. Matter **27** 425602
 Phien H N, Vidal G and McCulloch I P 2012 Phys. Rev. B **86** 245107
 Milsted A, Haegeman J, Osborne T J and Verstraete F 2013 Phys. Rev. B **88** 155116
 - [19] T. Numasawa *in preperation*
 - [20] Eisler V and Peschel I 2008 Ann. Phys. (Berlin) **17** 410
 - [21] Anous T, Hartman T, Rovai A and Sonner J 2016 JHEP **07** 123
 - [22] Mezei M and Stanford D 2016 arXiv:1608.05101
 - [23] Magan J M 2016 arXiv:1601.04663
 Jansen A and Magan J M 2016 arXiv:1604.03772
 - [24] N. Lashkari, J. Lin, H. Ooguri, B. Stoica and M. Van Raamsdonk, arXiv:1605.01075
 - [25] Sarosi G and Ugajin T 2016 JHEP **07** 114
 - [26] Blanco D D, Casini H, Hung L Y and Myers R C 2013 JHEP **1308** 060
 - [27] Cardy J and Tonni E arXiv:1608.01283
 - [28] Caputa P *in preperation*
 - [29] Bhattacharya J, Nozaki M, Takayanagi T and Ugajin T 2013 Phys. Rev. Lett. **110** 091602
 - [30] Giovannetti V, Montangero S and Fazio R 2008 Phys. Rev. Lett. **101** 180503
 Pfeifer R N C, Evenbly G and Vidal G 2009 Phys. Rev. A **79** 040301
 Evenbly G, Corboz P and Vidal G 2010 Phys. Rev. B **82** 132411
 Evenbly G and Vidal, G 2013 Quantum criticality with the multi-scale entanglement renormalization ansatz. In: Avella, A., Mancini, F. (eds.) Strongly correlated systems: numerical methods. Springer, Heidelberg, arXiv:1109.5334
 - [31] Lieb E, Schultz T and Mattis D, 1961 Ann. Phys., NY **16** 407
 Katsura S, 1962 Phys. Rev. **12** 71508
 Pfeuty P, 1970 Ann. Phys. **57** 79
 - [32] Damski B, Rams M M 2014 J. Phys. A: Math. Theor. **47** 025303
 - [33] Peschel I 2003 J. Phys. A: Math.Gen. **36** L205
 Vidal G, Latorre J I, Rico E and Kitaev A 2003 Phys. Rev. Lett. **90** 227902
 Jin B-Q and Korepin V E 2004 J. Stat. Phys. **116** 79
 Peschel I and Eisler V 2009 J. Phys. A: Math. Theor. **42** 504003